KICS The Korean Institute of Communications and Information Sciences

Available online at www.sciencedirect.com
ScienceDirect

ICT Express 9 (2023) 601–607

www.elsevier.com/locate/icte

Outage and capacity analysis of NOMA systems over dual-hop mixed powerline-wireless channels

Basem M. ElHalawany[a,b], Ahmed Samir[a], Mohamed Elsayed[a], Wali Ullah Khan[c], Kaishun Wu[b], Ehab Mahmoud Mohamed[d,e,*]

[a] *Faculty of Engineering at Shoubra, Benha University, Cairo, 11241, Egypt*
[b] *School of Computer Science, Shenzhen University, Shenzhen, 11241, China*
[c] *Interdisciplinary Centre for Security, Reliability and Trust (SnT), University of Luxembourg, Luxembourg City, 1855, Luxembourg*
[d] *College of Engineering, Prince Sattam Bin Abdulaziz University, Wadi Aldwaser, Saudi Arabia*
[e] *Aswan University, Aswan, Egypt*

Received 18 January 2022; received in revised form 17 May 2022; accepted 30 May 2022
Available online 6 June 2022

Abstract

Non-orthogonal multiple access (NOMA) has emerged as a promising technology for 5G networks and beyond. In order to fully reap the benefits of NOMA, it is essential to characterize its performance under different channel fading. In this paper, we carry out a performance analysis of the downlink NOMA-based dual-hop mixed powerline/wireless communication (PLC/WLC) system. Specifically, we investigate the system reliability and spectrum efficiency in terms of the outage probability and the ergodic capacity, respectively, where the PLC link undergoes lognormal fading while the WLC link undergoes block Rayleigh fading. The accuracy of the analytical results has been validated, the effect of different system controlling parameters is tested; and the optimal values of power allocation factors are obtained. Also, the system performance is compared to a benchmark system through representative extensive simulations.
© 2022 The Author(s). Published by Elsevier B.V. on behalf of The Korean Institute of Communications and Information Sciences. This is an open access article under the CC BY-NC-ND license (http://creativecommons.org/licenses/by-nc-nd/4.0/).

Keywords: Outage probability; Ergodic capacity; Non-orthogonal multiple access; Dual-hop relaying; Hybrid powerline-wireless

1. Introduction

Recently, powerline communication (PLC) technology has been considered for enabling data transfer over already deployed electrical power lines. One promising application of such technology is for smart grid networks, where communication can be established between consumer-end home area networks and transmission and distribution networks. Additionally, PLC can be efficiently used for enabling local area networks, home automation, and the Internet of Things (IoT) using the indoor wiring infrastructure [1]. Additionally, PLC could solve the penetration loss problem of wireless communication links that occurs when wireless signals go through walls and metallic structures. The main advantage of PLC lies in the significant reduction of deployment costs and the wide-spread access in buildings everywhere. Technically speaking, PLC works by superimposing high-frequency information signals, in the range of a few hundred Hz to hundreds of megahertz, over the low-frequency electrical power carriers to reuse the existing power lines for communication purposes [2–4]. However, to accomplish reliability for beyond fifth generation (B5G) and 6G networks, flexible, heterogeneous, and hybrid architectures are necessary to harness the benefits of different communication technologies to cover all possible scenarios.

Several studies investigated the coexistence of PLC links in conjunction with other communication links such as visible-light communication (VLC) and wireless communication links [5–10]. The authors in [5] investigated the performance of a dual-hop powerline/wireless communication (PLC/WLC) system through deriving closed-form expressions of the outage probability (OP), bit error rate (BER), and the ergodic capacity (EC). The PLC and wireless channels were modeled by lognormal and Rayleigh fading distributions, respectively. In [6], the authors presented an effective solution to protect the hybrid PLC/WLC system from malicious attacks by utilizing the physical characteristics of PLC channels. In [7], a

* Corresponding author at: College of Engineering, Prince Sattam Bin Abdulaziz University, Wadi Aldwaser, Saudi Arabia.
E-mail address: ehab_mahmoud@aswu.edu.eg (E.M. Mohamed).
Peer review under responsibility of The Korean Institute of Communications and Information Sciences (KICS).

https://doi.org/10.1016/j.icte.2022.05.010
2405-9595/© 2022 The Author(s). Published by Elsevier B.V. on behalf of The Korean Institute of Communications and Information Sciences. This is an open access article under the CC BY-NC-ND license (http://creativecommons.org/licenses/by-nc-nd/4.0/).

power allocation problem for a hybrid system composed of a cascaded PLC/VLC link in parallel to an RF wireless link is investigated. In [8], the authors derived an approximate closed-form expression of the average BER and an exact closed-form expression of the OP under a Nakagami-m distributed WLC link, while the PLC link is characterized by the lognormal distribution and Bernoulli-Gaussian noise. Similar to [8], the authors in [9] derived the average BER for the same system model and channel assumptions. However, they used the Gamma approximation to avoid the complication of using the exact lognormal distribution. Additionally, the authors in [10] considered an amplify and forward (AF) relaying over hybrid PLC/WLC architecture, where a Nakagami-m wireless fading and lognormal power line fading are used.

On the other hand, non-orthogonal multiple access (NOMA) technology is capable of boosting the communication system capacity [11] by allowing many users to non-orthogonally share the available resources at the expense of more complicated receivers. There are many categories of NOMA according to the multiplexing method, while the most widely used one is power domain-NOMA (PD-NOMA) [12,13], in which the multiplexing is carried out by superimposing users' information with different power levels. The PD-NOMA receiver employs successive interference cancellation (SIC) for decoding messages of higher power users before detecting its own message.

Hybrid PLC/WLC system that utilizes orthogonal multiple access (OMA) as a multiplexing technique has been studied in many research, but to the best of the authors' knowledge, the coexistence of NOMA and hybrid PLC/WLC has not been investigated before. In this work, we provide an analytical study for investigating the performance of NOMA-based dual-hop hybrid PLC/WLC communication systems with a decode-and-forward (DF) relay. The contributions of this paper can be listed as follows: (1) Derive closed-form expressions for the outage probabilities (OPs) besides analyzing the diversity order assuming that the wireless channels are characterized by block Rayleigh fading with additive white Gaussian noise (AWGN), while the PLC channel is characterized by Log-normal distribution with Bernoulli Gaussian noise. (2) Derive approximate expressions for the ergodic capacities (ECs). (3) Validate the analysis via extensive representative Monte-Carlo simulations. (4) Study the impact of system parameters on the performance and obtain the optimal power allocation factor. (5) Compare the performance of the proposed system with OMA as a benchmark.

The rest of the paper is organized as follows. The system model is introduced in Section 2. The analytical outage probabilities and ergodic capacities are derived in Sections 3 and 4 respectively. The proposed optimal power allocation algorithm is proposed in Section 5. Analytical and simulation results are discussed in Section 6 and our conclusions are provided in Section 7.

2. System model

In this work, we consider a NOMA-based mixed dual-hop relaying system, at which a source (S) exploits NOMA to transmit information to two wireless users (far user D_1 and near user D_2) via an intermediate hybrid DF multi-modal relay node (R). The relay is capable of receiving over a PLC link (h_P) from the source, then broadcast the reconstructed message over wireless links (h_1 and h_2) as shown in Fig. 1. We assume that a perfect channel state information (CSI) is available at R, D_1 and D_2. The source-to-relay PLC link undergoes a log-normal fading [9] and Bernoulli Gaussian noise (BGN), while the wireless links undergo a block Rayleigh fading with AWGN noise, where the channel coefficients are constant for each transmission block but vary independently between different blocks. Following the two-phases DF relaying protocol, at the first phase, S transmits the symbol X_s through the PLC channel to R, given that $x_S = \sqrt{\alpha P_S}\ S_1 + \sqrt{(1-\alpha)\ P_S} S_2$, without loss of generality the source assign the higher power allocation factor ($0.5 < \alpha < 1$) to the far user D_1, S_i to represent the information-bearing symbol transmitted from the BS to D_i with expectation $E\{|S_i|^2\} = 1$ for $i \in \{1, 2\}$, and P_s is the source total transmit power. The received signal at R can be expressed as

$$y_R = h_P\ e^{-\theta\ d_P}\ x_S + n_R, \tag{1}$$

where $\theta = a_0 + a_1\ f^k$ represents the attenuation over the PLC link, a_0 and a_1 are measurement-based constants, f is the operating frequency, k is the attenuation factor exponent [14], and d_P is the distance between S and R, n_R is a BGN with $n_R \sim \mathcal{CN}(0,\ \sigma_P^2)$ where $CN(0,\ \sigma^2)$ stands for the complex Gaussian distribution having zero mean and σ^2 as variance. Following NOMA principles, R decodes the strong message S_1 firstly while treating S_2 as interference, then applies SIC to decode S_2. Consequently, the signal-to-interference-plus noise ratios (SINRs) for detecting S_1 and S_2 are given as follows

$$\begin{aligned} \gamma_R^1 &= \frac{\rho_S\,\alpha\, e^{-2\theta d_P}|h_P|^2}{\rho_S\,(1-\alpha)\, e^{-2\theta d_P}|h_P|^2+1}, \\ \gamma_R^2 &= \rho_S\,(1-\alpha)\, e^{-2\theta d_P}|h_P|^2, \end{aligned} \tag{2}$$

where $\rho_S = \frac{P_S}{\sigma_P^2}$. During the second phase, R combines the two detected symbols using a second power allocation factor, β[1], such that $0.5 < \beta < 1$, where $x_R = \sqrt{\beta P_R}\ S_1 + \sqrt{(1-\beta)\ P_R} S_2$ and P_R is the relay transmit power. Then R broadcasts x_R over the wireless channels (h_1 and h_2) to D_1 and D_2, where the signals received at both destinations are given as follows

$$y_D^i = h_i\ d_i^{-v/2}\ x_R + n_i, \ \text{ for } i \in \{1, 2\} \tag{3}$$

where d_i is the normalized distance from R to D_i with respect to the cell radius, v is wireless channel path-loss exponent, n_i is the AWGN at D_i with $n_i \sim \mathcal{CN}(0,\ \sigma_o^2)$. Both destinations follow downlink NOMA detection, where D_1 directly decodes its intended symbol (S_1) directly since it is allocated higher power. The SINR for detecting S_1 at D_1 is given as follows

$$\gamma_{D1}^1 = \frac{\rho_R\,\beta\, d_1^{-v}|h_1|^2}{\rho_R\,(1-\beta)\, d_1^{-v}|h_1|^2+1}, \tag{4}$$

[1] It is noteworthy that for simplicity, the same power allocation factor, α, can be used. However, using another factor increases the degree of freedoms to improve the system performance.

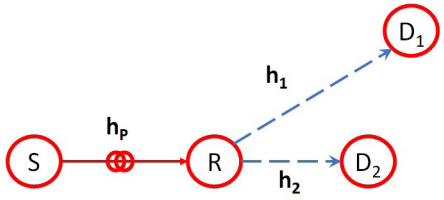

Fig. 1. A dual-hop mixed powerline-wireless system.

while D_2 decodes S_1 first which is followed by using SIC to detect S_2. The SINRs for detecting S_1 and S_2 at D_2 are given as follows

$$\begin{aligned}\gamma^1_{D2} &= \frac{\rho_R\,\beta\,d_2^{-v}|h_2|^2}{\rho_R\,(1-\beta)\,d_2^{-v}|h_2|^2+1},\\ \gamma^2_{D2} &= \rho_R\,(1-\beta)\,d_2^{-v}|h_2|^2,\end{aligned} \tag{5}$$

where $\rho_R = \frac{P_R}{\sigma_o^2}$.

3. Outage probability analysis

In this section, we derive the outage probabilities at both destinations and the system OP using (2), (4), and (5), which are given as follows

$$\begin{aligned} OP_1 &= 1-\Pr(\gamma^1_R>\pi_1,\gamma^1_{D1}>\pi_1) \overset{(a)}{=} 1-P_1(\pi_1)\;P_2(\pi_1),\\ OP_2 &= 1-\Pr(\gamma^1_R>\pi_1,\;\gamma^2_R>\pi_2,\gamma^1_{D2}>\pi_1,\text{`}\gamma^2_{D2}>\pi_2),\\ &\overset{(b)}{=} 1-P_3(\pi_1,\pi_2)\;P_4(\pi_1,\pi_2),\\ OP_{sys} &= 1-\Pr\left(\gamma^1_R>\pi_1,\gamma^1_{D1}>\pi_1,\;\gamma^2_R>\pi_2,\right.\\ &\qquad \left.\gamma^1_{D2}>\pi_1,\text{`}\gamma^2_{D2}>\pi_2\right),\\ &\overset{(c)}{=} 1-P_2(\pi_1)\;P_3(\pi_1,\pi_2)\;P_4(\pi_1,\pi_2),\end{aligned} \tag{6}$$

where $\pi_i = 2^{2R_i}-1$ is the threshold SNR, R_i is the normalized threshold rate for D_i, (a),(b), and (c) stem from the decorrelation of the random variables, and

$$\begin{aligned} P_1(\pi_1) &= \Pr(\gamma^1_R>\pi_1),\\ P_2(\pi_1) &= \Pr(\gamma^1_{D1}>\pi_1),\\ P_3(\pi_1,\pi_2) &= \Pr(\gamma^1_{D2}>\pi_1,\gamma^2_{D2}>\pi_2),\\ P_4(\pi_1,\pi_2) &= \Pr(\gamma^1_R>\pi_1,\gamma^2_R>\pi_2).\end{aligned} \tag{7}$$

In the following, we introduce the channel statistics of the involved channels and derive the closed-form expressions of P_1, P_2, P_3 and P_4, respectively.

Channels' Statistics: The amplitude of the PLC channel (h_P) is distributed according to log-normal distribution, $hp \sim \mathcal{LN}(\mu_{h_P},\ \sigma^2_{h_P})$, where μ_{h_P} is the mean and $\sigma^2_{h_P}$ is the variance. Consequently, the channel gain, $|h_P|^2$ follows a log-normal distribution, $|h_P|^2 \sim \mathcal{LN}(\mu',\ \sigma'^2)$, where $\mu' = 2\mu_{h_P}$ and $\sigma'^2 = 4\sigma^2_{h_P}$ [9]. The cumulative distribution function of the channel gain, $F_{|h_P|^2}(x)$, is given as follows:

$$F_{|h_P|^2}(x) = Q\left(\tfrac{\mu'-\ln(x)}{\sigma'}\right) = 1-Q\left(\tfrac{\ln(x)-\mu'}{\sigma'}\right), \tag{8}$$

where $Q(.)$ is the Gaussian Q-function [15]. On the other hand, the two wireless links, h_i, $i\in\{1,2\}$, undergo block Rayleigh fading distribution, which means that the channel gains, $|h_i|^2$ follow exponential distributions, $|h_i|^2 \sim exp(1)$, whose CDF is given as follows:

$$F_{|h_i|^2}(x) = 1-e^{-x}. \tag{9}$$

Derivation of P_1: Using (2), (7), and (8), P_1 can be expressed as $P_1 = \Pr\left(|h_P|^2 > \frac{\pi_1 e^{2\theta d_P}}{\rho_S\ \epsilon}\right)$, which can be reformulated as

$$P_1(\pi_1) \overset{(d)}{=} \begin{cases} Q\left(\frac{\ln(\frac{\pi_1 e^{2\theta d_P}}{\rho_S\ \epsilon})-\mu'}{\sigma'}\right), & \alpha > L_1\\ 0, & \alpha < L_1,\end{cases} \tag{10}$$

where $L_1 = \pi_1/(1+\pi_1)$, $\epsilon = \alpha(1+\pi_1)-\pi_1$ and (d) stems from using the CDF of $|h_P|^2$ in (8).

Derivation of P_2: Using (4), (7), and (9), P_2 can be expressed as $P_2 = \Pr\left(|h_1|^2 > \frac{\pi_1 d_1^v}{\rho_R\ \kappa}\right)$, which can be reformulated as

$$P_2(\pi_1) \overset{(e)}{=} \begin{cases} P_{21} = e^{\frac{-\pi_1 d_1^v}{\rho_R\ \kappa}}, & \beta > L_1\\ 0, & \text{Otherwise},\end{cases} \tag{11}$$

where $\kappa = \beta(1+\pi_1)-\pi_1$ and (e) stems from using the CDF of $|h_1|^2$ in (9).

Derivation of P_3: Using (5), (7), and (9), P_3 can be expressed as $P_3 = \Pr\left(|h_2|^2 > \frac{\pi_1 d_2^v}{\rho_R\ \kappa},\ |h_2|^2 > \frac{\pi_2 d_2^v}{\rho_R(1-\beta)}\right)$, which can be reformulated as

$$P_3(\pi_1,\pi_2) \overset{(f)}{=} \begin{cases} P_{31} = e^{\frac{-\pi_1 d_2^v}{\rho_R\kappa}}, & L_1<\beta<L_2\\ P_{32} = e^{\frac{-\pi_2 d_2^v}{\rho_R(1-\beta)}}, & \beta > L_2\\ 0, & \text{Otherwise},\end{cases} \tag{12}$$

where $L_2 = \pi_1(1+\pi_2)/(\pi_1+\pi_2(1+\pi_1))$ and (f) stems from using the CDF of $|h_2|^2$ in (9).

Derivation of P_4: Using (2), (7), and (8), P_4 can be expressed as $P_4(\pi_1,\pi_2) = \Pr\left(|h_P|^2 > \frac{\pi_1 e^{2\theta d_P}}{\rho_S\ \epsilon},\ |h_P|^2 > \frac{\pi_2 e^{2\theta d_P}}{\rho_S(1-\alpha)}\right)$, which can be reformulated as

$$P_4(\pi_1,\pi_2) \overset{(g)}{=} \begin{cases} P_{41} = Q\left(\frac{\ln(\frac{\pi_1 e^{2\theta d_P}}{\rho_S\ \epsilon})-\mu'}{\sigma'}\right), & L_1<\alpha<L_2\\ P_{42} = Q\left(\frac{\ln(\frac{\pi_2 e^{2\theta d_P}}{\rho_S(1-\alpha)})-\mu'}{\sigma'}\right), & \alpha > L_2\\ 0, & \text{Otherwise},\end{cases} \tag{13}$$

where (g) stems from using the CDF of $|h_P|^2$ in (8). By substituting (10), (11), (12), and (13) into (6), we obtain closed form expressions for OP_1, OP_2, and OP_{sys}.

Diversity Order: To obtain deep insights regarding our system, we derive the diversity order of the outage probabilities in (6), where the diversity order is defined as the slope of those curves. Using [16,17], we can calculate diversity orders as $d^m_{OP} = -\lim_{\rho\to\infty}(\log(OP^\infty_m)/\log(\rho))$, where $m\in\{1,2,sys\}$ and OP^∞_m is OP_m when ρ tends to ∞, which can be calculated by finding P^∞_i for $i\in\{1,2,3,4\}$ as follows:

$$P^\infty_1 = \begin{cases} \frac{\sigma' e^{-\frac{(\ln(\frac{\pi_1 e^{2\theta d_p}}{\rho_S\varepsilon})-\mu')^2}{2\sigma'^2}}}{\sqrt{2\pi}(\ln(\frac{\pi_1 e^{2\theta d_p}}{\rho_S\varepsilon})-\mu')}, & \alpha > L_1\\ 0, & Otherwise\end{cases} \tag{14}$$

$$P_2^{\infty} = \begin{cases} 1 - \frac{\pi_1 d_1^v}{\rho_R k}, & \beta > L_1 \\ 0, & Otherwise \end{cases} \tag{15}$$

$$P_3^{\infty} = \begin{cases} 1 - \frac{\pi_1 d_2^v}{\rho_R k}, & L_1 < \beta < L_2 \\ 1 - \frac{\pi_2 d_2^v}{\rho_R (1-\beta)}, & \beta > L_2 \\ 0, & Otherwise \end{cases} \tag{16}$$

$$P_4^{\infty} = \begin{cases} \frac{e^{-\frac{(\ln(\frac{\pi_1 e^{2\theta d_p}}{\rho_s \varepsilon}) - \mu')^2}{2\sigma'^2}}}{\sqrt{2\pi}(\ln(\frac{\pi_1 e^{2\theta d_p}}{\rho_s \varepsilon}) - \mu')}, & L_1 < \alpha < L_2 \\ \frac{e^{-\frac{(\ln(\frac{\pi_2 e^{2\theta d_p}}{\rho_s (1-\alpha)}) - \mu')^2}{2\sigma'^2}}}{\sqrt{2\pi}(\ln(\frac{\pi_2 e^{2\theta d_p}}{\rho_s (1-\alpha)}) - \mu')}, & \alpha > L_2 \\ 0, & Otherwise \end{cases} \tag{17}$$

Taking into consideration (14), (15), (16), (17), and some simple mathematical expressions, the diversity order $d_{OP}^m \propto \rho^{-1}$, which means that $d_{OP}^m = 1$. This result coincides with the plots in Fig. 3 at Section 6.

4. Ergodic capacity analysis

In this section, we investigate the ergodic capacity of the considered system. The instantaneous capacities for both users are given by [18] as

$$\begin{aligned} C_1 &= \tfrac{1}{2}\log\big(1 + \min(\gamma_R^1, \gamma_{D1}^1, \gamma_{D2}^1)\big) \\ C_2 &= \tfrac{1}{2}\log\big(1 + \min(\gamma_R^2, \gamma_{D2}^2)\big) \end{aligned} \tag{18}$$

Consequently, the ergodic sum capacity of the system can be formulated as $ESC = EC_{S_1} + EC_{S_2}$, where EC_{S_i} for $i \in \{1, 2\}$ is the expectation of the channel capacity as follows [18]

$$EC_{S_i} = \frac{1}{2\ln 2}\int_{\pi=0}^{\infty} \frac{1}{1+\pi}\big[1 - F_{\gamma_i}(\pi)\big]d\pi. \tag{19}$$

Ergodic Capacity of D_1: The CDF $F_{\gamma_1}(\pi)$ can be written as

$$\begin{aligned} F_{\gamma_1}(\pi) &= 1 - pr(\gamma_R^1 > \pi, \gamma_{D1}^1 > \pi, \gamma_{D2}^1 > \pi) \\ &\overset{(h)}{=} 1 - P_1(\pi)\ P_2(\pi)\ P_5(\pi), \end{aligned} \tag{20}$$

where (h) stems from the decorrelation of the random variables, and $P_5(\pi) = pr(\gamma_{D2}^1 > \pi)$, which is reformulated as

$$P_5(\pi) = \begin{cases} e^{-\frac{\gamma d_2^v}{\rho_R k}}, & \beta > \frac{\pi}{1+\pi} \\ 0, & otherwise \end{cases}. \tag{21}$$

By substituting from (10), (11), and (21) into (19), EC_{S_1} can be formulated as

$$EC_{S_1} = \frac{1}{2\ln 2}\int_{\pi=0}^{\frac{\alpha}{1-\alpha}} \frac{e^{-\frac{\pi(d_1^v + d_2^v)}{\rho_R k}}}{1+\pi} Q\left(\frac{\ln(\frac{\pi e^{2\theta d_p}}{\rho_s \varepsilon}) - \mu'}{\sigma'}\right)d\pi, \tag{22}$$

However, to the best of our knowledge, there is no closed-form expression for such intractable integration. In the following, we provide an approximation using Gauss–Laguerre quadrature [19] by introducing the following variable transformation, where $\tau = \pi(d_1^v + d_2^v)/\rho_R k$. Consequently, we can express EC_{S_1} as

$$EC_{S_1} = \frac{1}{2\ln 2}\int_{\tau=0}^{\infty} e^{-\tau} f_1(\tau)d\tau, \tag{23}$$

where,

$$f_1(\tau) = \frac{\alpha \rho_R d\, Q(\frac{\ln(\frac{\rho_R \tau e^{2\theta d_p}}{\rho_s d}) - \mu'}{\sigma'})}{(d + \rho_R \tau)(d + (1-\alpha)\rho_R \tau)}. \tag{24}$$

Using [[19], eq. (25.4.45)], we can express the approximated value as

$$EC_{S_1} \approx \frac{1}{2\ln 2}\sum_{i=1}^{n} w_i f_1(\tau_i), \tag{25}$$

where τ_i is the ith zero of the Laguerre polynomial, $L_n(\tau)$, while w_i is the weights that can be calculated as follows:

$$w_i = \frac{(n!)^2 \tau_i}{(n+1)^2 [L_{n+1}(\tau_i)]^2} \tag{26}$$

Ergodic Capacity of D_2: Similar to EC_{S_1}, the CDF of γ_2 can be expressed as

$$F_{\gamma_2}(\pi) = 1 - pr(\gamma_R^2 > \pi, \gamma_{D2}^2 > \pi) = 1 - P_6(\pi)\ P_7(\pi) \tag{27}$$

where

$$\begin{aligned} P_6 &= pr(\gamma_R^2 > \pi) = Q(\tfrac{\ln(\frac{e^{2\theta d_p \pi}}{(1-\alpha)\rho_s}) - \mu'}{\sigma'}) \\ P_7 &= pr(\gamma_{D2}^2 > \pi) = e^{-\frac{d_2^v \pi}{(1-\alpha)\rho_R}}. \end{aligned} \tag{28}$$

By Substituting from (28) into (19) then

$$\begin{aligned} EC_{S_2} &= \frac{1}{2\ln 2}\int_{\pi=0}^{\infty} \frac{e^{-\frac{d_2^v \pi}{(1-\alpha)\rho_R}}}{1+\pi} Q\left(\frac{\ln(\frac{e^{2\theta d_p \pi}}{(1-\alpha)\rho_s}) - \mu'}{\sigma'}\right)d\pi \\ &= \frac{1}{2\ln 2}\int_{\pi=0}^{\infty} e^{-\pi} \frac{e^{\pi - \frac{d_2^v \pi}{(1-\alpha)\rho_R}}}{1+\pi} Q\left(\frac{\ln(\frac{e^{2\theta d_p \pi}}{(1-\alpha)\rho_s}) - \mu'}{\sigma'}\right)d\pi, \end{aligned} \tag{29}$$

Eq. (29) can be approximated similar to (23) as [[19], eq. (25.4.45)]

$$EC_{S_2} \approx \frac{1}{2\ln 2}\sum_{i=1}^{n} w_i f_2(\pi_i) \tag{30}$$

where,

$$f_2(\pi) = \frac{e^{\pi - \frac{d_2^v \pi}{(1-\alpha)\rho_R}}}{1+\pi} Q\left(\frac{\ln(\frac{e^{2\theta d_p \pi}}{(1-\alpha)\rho_s}) - \mu'}{\sigma'}\right) \tag{31}$$

5. Proposed power allocation algorithm

In this section, we discuss a proposed power allocation algorithm for optimizing the outage probability of the system. The proposed optimization problem is given as follows:

$$\min_{\alpha,\beta}\ OP_{sys} \tag{32a}$$

$$\text{s.t. } 0.5 < \alpha < 1 \tag{32b}$$

$$0.5 < \beta < 1 \tag{32c}$$

In the following, we provide Theorem 1 to prove the convexity of the problem.

Theorem 1. *The problem in (32) is a convex optimization problem.*

Table 1
Parameter values used for simulations.

Parameter	σ' (dB)	μ'	α or β	π_i	ρ (dB)	f (kHz)	a_0	a_1	k	d_1	d_2	d_p	v
value used	2	1	0.5 : 0.99	1 : 2	0 : 30	500	$2.03e-3$	$3.75e-7$	0.7	2	1	10	3

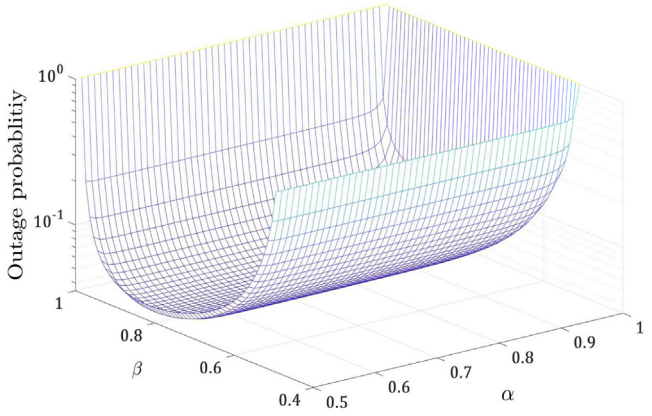

Fig. 2. The system OP versus power allocation factors (α and β) with ρ = 30 dB, $\pi_1 = 1$, and $\pi_2 = 2$.

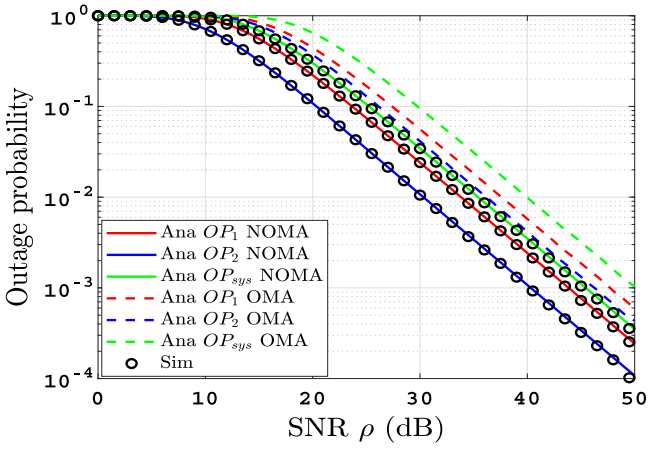

Fig. 3. OP versus SNR (ρ) with $R_1 = 0.5$, $R_2 = 0.75$, $\alpha = 0.6$, and $\beta = 0.83$.

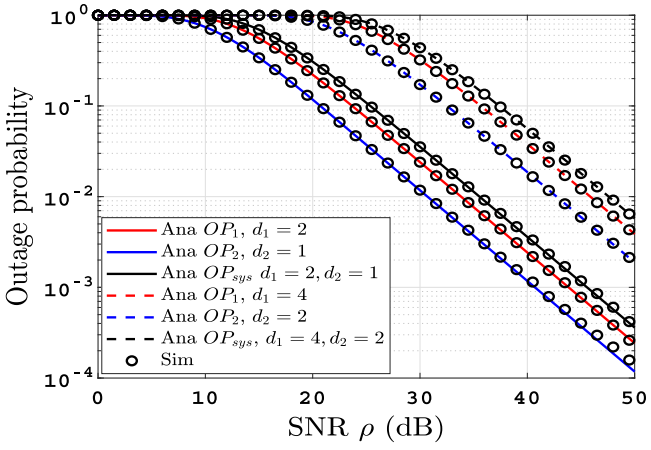

Fig. 4. OP versus SNR (ρ) when duplicates $d1$ and $d2$ while $\pi_1 = 1$, $\pi_2 = 2$, $\alpha = 0.6$, and $\beta = 0.83$.

Proof. Please, refer to Appendix.

Since (32) is a convex optimization problem, it can be solved using any commercial solver such as Matlab or Mathematica. With the system parameters setting defined in Table 1, we show the variations of the system OP as a function of both α and β in Fig. 2, to show the convexity graphically. The solution of such problem gives an optimal value for power allocation factors as $\alpha = 0.6$ and $\beta = 0.83$. This solution is used as an optimal power allocation scheme in all figures of outage in Section 6.1.

6. Discussions and results

In this section, we present representative numerical results to demonstrate the behavior of the system and to validate the derived expressions. Unless mentioned otherwise, the simulation parameters used in the plots are given in Table 1, which depend on [9,20,21]. The notation "Ana" is used for the exact analytical results of the OP and the approximated EC, and "Sim" denotes Monte-Carlo simulation results in all legends. We have assumed that $\rho_s = \rho_R = \rho$.

6.1. Outage probability results

Fig. 3 shows the variations of the OP at D_1, D_2, and OP_{sys} versus SNR (ρ) assuming $R_1 = 0.5$ bits/s/Hz and $R_2 = 0.75$ bits/s/Hz. The optimal values of the power allocation factors obtained from Section 5; $\alpha = 0.6$, and $\beta = 0.83$; have been used. The result shows that the exact and the simulation result coincide for the entire span of ρ which validates the analysis. Additionally, we note an improvement in OPs performance as ρ increases. To clarify the advantages of the proposed system in this work; the NOMA-based mixed dual-hop relaying system; against a well-known reference system, we compared our system with an OMA-based mixed dual-hop relaying system. Through the comparison held, it becomes clear to us the superiority of the proposed system due to the spectrum efficiency of NOMA. Since $OP_{sys} = 0.034$ at $\rho = 30$ dB and $OP_{sys} = 0.0034$ at $\rho = 40$ dB, so the diversity order can be calculated as $log(0.034) - log(0.0034) \approx 1$.

Under the same settings, Fig. 4 shows the effect of changing distance between end-users and relay on the OPs at both users and the system OP. The results show that the OPs degrade with the increase in distance due to the corresponding decrease in the received SINR.

Fig. 5 shows the variations of the OPs as functions of the power allocation factor in the range from 0.5 to 0.99 assuming $\alpha = \beta$, ρ = 30 dB, $\pi_1 = 1$, and $\pi_2 = 2$. The results show the improvement in OP at D_1 with increasing α as this leads to an increase in the power of its own message and in the same time reducing interference power from D_2. The situation of OP at D_2 witnesses a great reduction at the beginning until α reaches a certain value at which the curve inflicted and its OP starts to

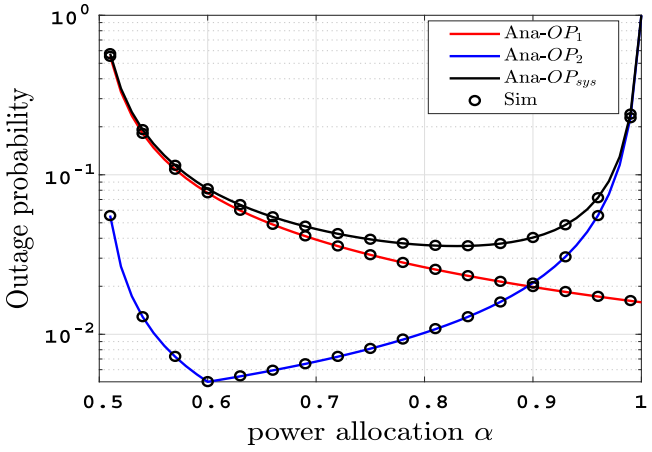

Fig. 5. OP versus power allocation factor (α or β) with ρ = 30 dB, $\pi_1 = 1$, and $\pi_2 = 2$.

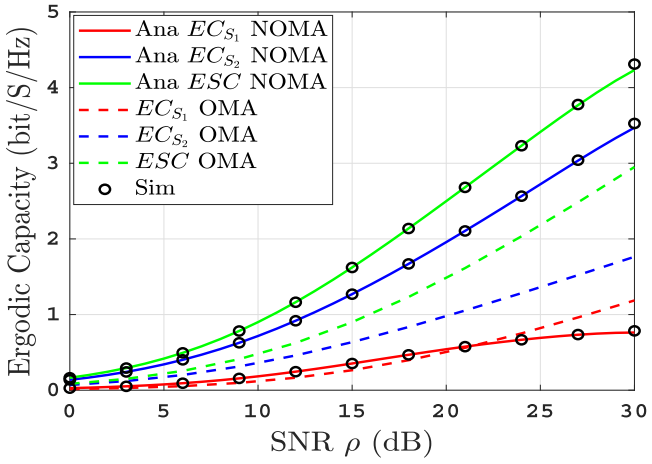

Fig. 6. The EC versus SNR (ρ) with $\alpha = \beta = 0.7$.

degrade. The reason behind this trend is that as α increases, the successful detection probability of S_1 enhanced which is a pre-request for implementing SIC at D_2. With the steady increase in value of α, the SINR for decoding the second message will go down below the required threshold and D_2 fails to detect its own message. Additionally, the system OP takes the same trend as OP at D_2.

6.2. Ergodic capacity results

Fig. 6 shows the EC for both users and the ESC against the transmit SNR. It is noteworthy that EC_{S_1} increases gradually at low-SNR region and saturates at the high-SNR due to the interference of the second user. On the other hand, EC_{S_2} increases with SNR with no saturation since we assume a perfect SIC scenario. Although the performance of EC for each message is different, the performance of ESC follows the trend of EC_{S_2}. Additionally, we compare the performance of the proposed NOMA-based system with an OMA-based system under the same parameter settings. The results show that the ESC of the NOMA-based system is better compared with the OMA-based one.

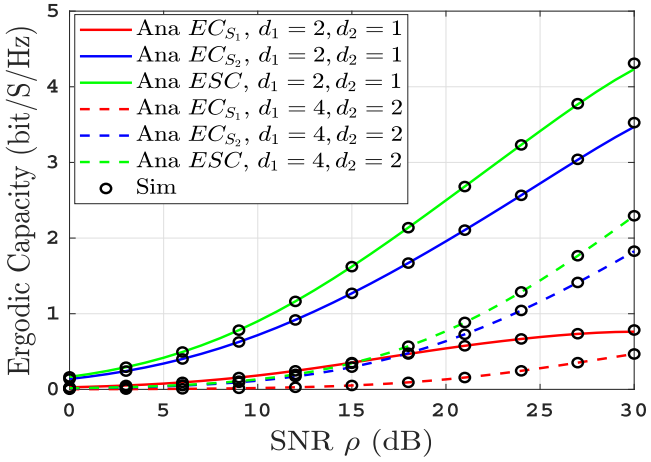

Fig. 7. EC versus SNR (ρ) when duplicates $d1$ and $d2$ while $\alpha = \beta = 0.7$.

To present the effect of changing distance between end-users and relay on the ECs, Fig. 7 shows the ECs under different settings of the distances d_1 and d_2. From the figure, it is clear that the capacities degrade while increasing the distance, also this is due to the decrease in the received SINR with the increase in distance.

7. Conclusion

Through this paper, we proposed a novel two-user NOMA-based dual-hop hybrid PLC/WLC system that uses a DF relay. The closed-form formulas for the OPs of both users and the system OP, the ECs for the two messages, the ESC, and the diversity order for the OPs were derived. Monte-Carlo simulations were used after that to confirm the accuracy of driven forms. Also, we investigated the effect of varying the distance between the end-users and the relay on the system performance. Also, we studied the impact of the power allocation factors on the system's OP performance and the existence of an optimal value under constant SNR. Also, we held a comparison between the proposed system in contrast with a well-known benchmark system to illustrate that our system can add a good contribution to the communication practical systems. As future research directions, we may find the optimal values of power allocation factors analytically.

CRediT authorship contribution statement

Basem M. ElHalawany: Conception and design of study, Drafting the manuscript, Revising the manuscript critically for important intellectual content, Analysis and/or interpretation of data. **Ahmed Samir:** Conception and design of study, Drafting the manuscript, Analysis and/or interpretation of data. **Mohamed Elsayed:** Conception and design of study, Analysis and/or interpretation of data, Drafting the manuscript. **Wali Ullah Khan:** Conception and design of study, Acquisition of data, Revising the manuscript critically for important intellectual content. **Kaishun Wu:** Conception and design of study, Revising the manuscript critically for important intellectual content. **Ehab Mahmoud Mohamed:** Conception and design of study, Acquisition of data, Revising the manuscript critically for important intellectual content.

Declaration of competing interest

The authors declare that they have no known competing financial interests or personal relationships that could have appeared to influence the work reported in this paper.

Acknowledgment

All authors approved the final version of the manuscript.

Appendix

In this appendix, a detailed derivation that proves the convexity of the problem is described in (32). The first step is to re-write the system OP as $OP_{sys} = 1 - I_{sys}$ for different intervals of α and β, where

$$I_{sys} = \begin{cases} I_1 = P_{21}P_{31}P_{41}, & L_1 < \alpha < L_2, L_1 < \beta < L_2 \\ I_2 = P_{21}P_{31}P_{42}, & \alpha > L_2, L_1 < \beta < L_2 \\ I_3 = P_{21}P_{32}P_{41}, & L_1 < \alpha < L_2, \beta > L_2 \\ I_4 = P_{21}P_{32}P_{42}, & \alpha > L_2, \beta > L_2 \\ 0, & otherwise. \end{cases} \tag{A.33}$$

To show the convexity, we need to show that the Hessian matrix (H) is positive semi-definite, where H_1 under the first region $L_1 < \alpha < L_2, L_1 < \beta < L_2$ is given as

$$H = \begin{bmatrix} \Delta_1 & \Delta_2 \\ \Delta_3 & \Delta_4 \end{bmatrix} = \begin{bmatrix} -\frac{\partial^2 I_1}{\partial \alpha^2} & -\frac{\partial^2 I_1}{\partial \alpha \partial \beta} \\ -\frac{\partial^2 I_1}{\partial \beta \partial \alpha} & -\frac{\partial^2 I_1}{\partial \beta^2} \end{bmatrix}. \tag{A.34}$$

Finding those derivatives we reach

$$\Delta_1 = \frac{(1+\pi_1)^2 e^{-\frac{c_1+c_2}{\kappa}}}{\varepsilon^2 \sigma'^3 \sqrt{2\pi}} e^{-\left(\frac{\ln \frac{c_3}{\varepsilon} - \mu'}{\sigma' \sqrt{2}}\right)^2} (\sigma'^2 - \ln \frac{c_3}{\varepsilon} + \mu'), \tag{A.35a}$$

$$\Delta_2 = \Delta_3 = -\frac{(c_1+c_2)(1+\pi_1)^2}{\varepsilon \kappa^2 \sigma' \sqrt{2\pi}} e^{-\frac{c_1+c_2}{\kappa}} e^{-\left(\frac{\ln \frac{c_3}{\varepsilon} - \mu'}{\sigma' \sqrt{2}}\right)^2}, \tag{A.35b}$$

$$\Delta_4 = \frac{\sigma'(1+\pi_1)^2 (c_1+c_2)^2 (1 - \frac{2\kappa}{c_1+c_2}) e^{-\frac{c_1+c_2}{\kappa}}}{\kappa^4 (\ln \frac{c_3}{\varepsilon} - \mu') \sqrt{2\pi}} e^{-\left(\frac{\ln \frac{c_3}{\varepsilon} - \mu'}{\sigma' \sqrt{2}}\right)^2}, \tag{A.35c}$$

where $c_1 = \pi_1 d_1^v / \rho_R$, $c_2 = \pi_1 d_2^v / \rho_R$ and $c_3 = \pi_1 e^{2\theta d_P} \rho_s$. As we can see that Δ_1; which is the first leading minor; is positive, and after some mathematical manipulation we can prove that $\Delta_1 \Delta_4 - \Delta_2 \Delta_3$; which is the second leading minor; is positive as well, which demonstrates the convexity of the proposed optimization problem. We can follow the same steps to prove the convexity over the other regions as well.

References

[1] G. Prasad, L. Lampe, Full-duplex power line communications: Design and applications from multimedia to smart grid, IEEE Commun. Mag. (2019) 2–8.

[2] IEEE standard for broadband over power line networks: Medium access control and physical layer specifications, 2010, pp. 1–1586, IEEE Std 1901-2010.

[3] IEEE draft standard for medium frequency (less than 15 MHz) power line communications for smart grid applications, 2018, pp. 1–232, IEEE P1901.1/D9.5, September 2017.

[4] IEEE standard for low-frequency (less than 500 kHz) narrowband power line communications for smart grid applications - amendment 1, 2015, pp. 1–28, IEEE Std 1901.2a-2015 (Amendment to IEEE Std 1901.2-2013).

[5] L. Yang, X. Yan, S. Li, D.B. da Costa, M.S. Alouini, Performance analysis of dual-hop mixed PLC/RF communication systems, 2020, pp. 1–8, arXiv, arXiv:2011.09051.

[6] H.N. Noura, R. Melki, A. Chehab, J.H. Fernandez, Efficient and robust data availability solution for hybrid PLC/RF systems, Comput. Netw. (2020) 107675.

[7] M. Kashef, M. Abdallah, N. Al-Dhahir, Transmit power optimization for a hybrid PLC/VLC/RF communication system, IEEE Trans. Green Commun. Netw 2 (1) (2018) 234–245.

[8] A. Mathur, M.R. Bhatnagar, Y. Ai, M. Cheffena, Performance analysis of a dual-hop wireless-power line mixed cooperative system, IEEE Access 6 (2018) 34380–34392.

[9] A. Mathur, M.R. Bhatnagar, B.K. Panigrahi, Performance of a dual-hop wireless-powerline mixed cooperative system, in: 2016 International Conference on Advanced Technologies for Communications, ATC, Hanoi, 2016, pp. 401–406.

[10] Z. Chen, Y. Jing, D. Han, L. Wang, Performance analysis of dual-media cooperative communication based on wireless and power line under hybrid fading, Int. J. Distrib. Sens. Netw. 15 (5) (2019) 1550147719850701.

[11] A.A. Amin, S.Y. Shin, Capacity enhancement of NOMA-MIMO with OAM-IM, IEEE Wirel. Commun. Lett. (2021) 1.

[12] M. Elsayed, A. Samir, A.A. El-Banna, X. Li, B.M. Elhalawany, When NOMA multiplexing meets symbiotic ambient backscatter communication: Outage analysis, IEEE Trans. Veh. Technol. (2021).

[13] B.M. ElHalawany, F. Jameel, D.B. da Costa, U.S. Dias, K. Wu, Performance analysis of downlink NOMA systems over κ-μ shadowed fading channels, IEEE Trans. Veh. Technol. 69 (1) (2020) 1046–1050.

[14] W. Gheth, K.M. Rabie, B. Adebisi, M. Ijaz, G. Harris, A. Alfitouri, Hybrid power-line/wireless communication systems for indoor applications, in: 2018 11th International Symposium on Communication Systems, Networks Digital Signal Processing, CSNDSP, 2018, pp. 1–6.

[15] P.A. ShirinAbadi, A. Abbasi, On approximation of Gaussian Q-function and its applications, in: 2019 IEEE 10th Annual Ubiquitous Computing, Electronics Mobile Communication Conference, UEMCON, 2019, pp. 0883–0887.

[16] B.M. ElHalawany, A.A.A. El-Banna, K. Wu, Physical-layer security and privacy for vehicle-to-everything, IEEE Commun. Mag. 57 (10) (2019) 84–90.

[17] S.M. Ibraheem, W. Bedawy, W. Saad, M. Shokair, Outage performance of NOMA-based DF relay sharing networks over nakagami-m fading channels, in: 2018 13th International Conference on Computer Engineering and Systems, ICCES, 2018, pp. 512–517.

[18] A. Rauniyar, P. Engelstad, O.N. Østerbø, Ergodic capacity performance of NOMA-SWIPT aided IoT relay systems with direct link, in: 2020 18th International Symposium on Modeling and Optimization in Mobile, Ad Hoc, and Wireless Networks, WiOPT, 2020, pp. 1–8.

[19] M. Abramowitz, I.A. Stegun, Handbook of Mathematical Functions with Formulas, Graphs, and Mathematical Tables, ninth Dover printing, tenth GPO printing, Dover, New York, 1964.

[20] A. Dubey, D. Sharma, R.K. Mallik, S. Mishra, Modeling and performance analysis of a PLC system in presence of impulsive noise, in: 2015 IEEE Power Energy Society General Meeting, 2015, pp. 1–5.

[21] A. Dubey, R.K. Mallik, R. Schober, Performance of a PLC system in impulsive noise with selection combining, in: 2012 IEEE Global Communications Conference, GLOBECOM, 2012, pp. 3508–3512.